# Higher hyperpolarization activated current ($I_h$) in a subpopulation of hippocampal stratum oriens CA1 interneurons in Fragile X mice.

**Lauren T. Hewitt and Darrin H. Brager**

**Department of Neuroscience, Institute for Neuroscience**
**University of Texas at Austin**
**Austin, TX 78712**

**Corresponding author:** Lauren T. Hewitt (laur.hewitt@utexas.edu)

**Running Title: Intrinsic excitability hippocampal interneurons in FX**

**Abstract**

Fragile X syndrome is the most common inherited form of intellectual disability and the leading monogenetic cause of autism. Studies in mouse models of autism spectrum disorders, including the Fmr1 knockout (FX) mouse, suggest that an imbalance between excitation and inhibition in hippocampal circuits contributes to behavioral phenotypes. In addition to changes in excitatory and inhibitory synaptic transmission, changes in the intrinsic excitability of neurons can also contribute to circuit dysfunction. We and others previously identified changes in multiple voltage-gated ion channels in hippocampal excitatory pyramidal neurons in FX mice. Whether the intrinsic properties of hippocampal inhibitory interneurons are altered in FX remains largely unknown. We made whole-cell current clamp recordings from three types of interneurons in stratum oriens of the hippocampus: fast-spiking cells and two classes of low threshold spiking cells, oriens-lacunosum moleculare (OLM) and low-threshold high $I_h$ (LTH) neurons. We found that in FX mice input resistance and action potential firing frequency were lower in LTH, but not FS or OLM, interneurons compared to wild type. LTH cell input resistance was not different between wild type and FX mice in the presence of the h-channel blocker ZD7288 suggesting a greater contribution of $I_h$ in FX LTH cells. In agreement, we found using voltage clamp recording that $I_h$ was higher in FX LTH cells compared to wild type. Our results suggest that the intrinsic excitability of LTH inhibitory interneurons contribute to altered excitatory/inhibitory balance in the hippocampus of FX mice.

## Significance statement

Changes in the balance between excitation and inhibition are believed to contribute to neurodevelopmental disorders. We, and others, previously identified changes in the intrinsic properties of excitatory hippocampal neurons in a mouse model of Fragile X syndrome. In this paper we use physiological and biochemical approaches to investigate inhibitory interneurons in the CA1 region of the hippocampus of the Fragile X mouse. We found that the hyperpolarization activated current $I_h$ is higher, which lowers the excitability of one specific type of interneuron. This study highlights how changes to voltage-gated ion channels in specific neuronal populations contribute to the reported altered excitatory/inhibitory balance in Fragile X syndrome.

## Introduction

Fragile X Syndrome (FXS) is the primary monogenetic cause of autism and the most common form of inherited intellectual disability. Patients with FXS exhibit epilepsy, sensory hypersensitivity, and anxiety among other cognitive impairments (Hagerman and Hagerman, 2002; Kaufmann et al., 2004; Hall et al., 2008; Hagerman et al., 2009). One working hypothesis is that disruption of the excitatory/inhibitory (E/I) balance in FXS impairs brain circuit function. Inhibitory interneuron activity is essential in maintaining the E/I balance in the brain. The hippocampus contains a diverse population of inhibitory interneurons that form distinct circuits that control the precise timing of excitatory activity in the hippocampus (Cobb et al., 1995; Freund and Buzsáki, 1996; Klausberger and Somogyi, 2008; DeFelipe et al., 2013). Changes in hippocampal inhibition, even at the single cell level, could play a crucial role in this imbalance

(Rubenstein and Merzenich, 2003; Belmonte and Bourgeron, 2006; Chao et al., 2010; Paluszkiewicz et al., 2011a).

FXS is characterized by hypermethylation and transcriptional silencing of the *Fmr1* gene (Fu et al., 1991) leading to a loss of Fragile X Messenger Ribonucleoprotein 1 (formerly known as Fragile X Mental Retardation Protein, FMRP) ((Bell et al., 1991), FMR1 gene ID: 2332, NCBI, 2022). FMRP is highly expressed in the hippocampus in excitatory pyramidal neurons (Feng et al., 1997); however, currently there are publications that describe FMRP expression in somatostatin interneurons in the cortex (Paluszkiewicz et al., 2011b), but there are currently no reports of the co-expression of FMRP with specific subtypes of inhibitory interneurons in the CA1 hippocampus. FMRP regulates the function and expression of voltage-gated ion channels in excitatory pyramidal neurons and changes were identified in voltage-gated ion-channels in hippocampal pyramidal cells from Fmr1 KO mice (Brager et al., 2012; Routh et al., 2013; Contractor et al., 2015; Deng and Klyachko, 2016; Deng et al., 2019; Brandalise et al., 2020). It is currently unknown how the loss of FMRP affects hippocampal inhibitory interneurons. Therefore, to fully understand changes in E/I balance in the hippocampus in FXS, it is essential to understand how the loss of FMRP alters the intrinsic cellular excitability of specific inhibitory interneurons.

CA1 stratum oriens interneurons can be divided into two canonical interneuron types based on action potential firing: fast spiking (FS) and low threshold spiking (LTS). FS neurons exert strong, feedforward inhibition onto CA1 pyramidal cell bodies while LTS neurons exert feedback inhibition onto CA1 pyramidal cell dendrites (Klausberger and

Somogyi, 2008). We recently showed that LTS neurons could be further divided into two distinct classes: Oriens Lacunosum Moleculare (OLM) neurons and Low Threshold High $I_h$ (LTH) neurons (Hewitt et al., 2021). In this study, we used patch clamp electrophysiology to investigate differences in CA1 stratum oriens interneurons between wild type and FX mice. We found no significant differences in input resistance and action potential firing frequency in FS and OLM neurons between wild type and FX mice. In contrast, input resistance and action potential firing frequency were significantly lower in LTH neurons from FX mice compared to wild type. Previous studies showed that the intrinsic excitability of excitatory neurons is altered by changes in HCN channels ($I_h$) in a cell-type specific manner in FX mice (Brager et al., 2012; Zhang et al., 2014; Kalmbach et al., 2015; Brandalise et al., 2020). Given that LTH neurons have a relatively higher expression of HCN channels ($I_h$) compared to OLM cells (Hewitt et al., 2021), we tested the hypothesis that higher $I_h$ contributes to the lower intrinsic excitability of FX LTH neurons. In agreement with this hypothesis, we found that the effect of $I_h$ blocker ZD7288 on LTH neuron input resistance was higher in FX mice compared to wild type. Furthermore, direct measurement of $I_h$ using voltage-clamp recordings found that the amplitude of $I_h$ in LTH neurons was higher in FX compared to wild type.

## Methods

### Slice preparation:

The University of Texas at Austin Institutional Animal Care and Use Committee approved all animal procedures. Mice had free access to food and water and were

housed in a reverse light-dark cycle of 12 hr on/ 12 hr off. Experiments used male 2-4 month old wild-type and *fmr1*$^{-/y}$ (FX) mice on a C57/Bl6 background. Mice were anesthetized using a ketamine/xylazine cocktail (100/10 mg/kg) and then underwent cardiac perfusions with ice-cold saline consisting of (in mM): 2.5 KCl, 1.25 $NaH_2PO_4$, 25 $NaHCO_3$, 0.5 $CaCl_2$, 7 $MgCl_2$, 7 dextrose, 205 sucrose, 1.3 ascorbate acid, and 3 sodium pyruvate (bubbled constantly with 95% $O_2$/5% $CO_2$ to maintain pH at ~7.4). The brain was removed and sliced into 300 µM parasagittal sections from the middle hippocampus using a vibrating tissue slicer (Vibratome 300, Vibratome Inc). The slices were placed in a chamber filled with artificial cerebral spinal fluid (aCSF) consisting of (in mM): 125 NaCl, 2.5 KCl, 1.25 $NaH_2PO_4$, 25 $NaHCO_3$, 2 $CaCl_2$, 2 $MgCl_2$, 10 dextrose, 1.3 ascorbic acid and 3 sodium pyruvate (bubbled constantly with 95% $O_2$/5% $CO_2$) for 30 minutes at 35°C and then held at room temperature until time of recording.

**Electrophysiology**

Slices were placed in a submerged, heated (33-34 C°) recording chamber and continually perfused with aCSF (in mM): 125 NaCl, 3 KCl, 1.25 $NaH_2PO_4$, 25 $NaHCO_3$, 2 $CaCl_2$, 1 $MgCl_2$, 10 dextrose, and 3 sodium pyruvate (bubbled constantly with 95% $O_2$/5% $CO_2$). Synaptic transmission was blocked with 20 µM DNQX, 25 µM D-AP5, and 2 µM Gabazine. The stratum oriens region of CA1 in slices were visualized with a Zeiss AxioScope or AxioExaminer under 60x magnification.

Current clamp recordings were made using a Dagan BVC-700 amplifier and custom written acquisition software using Igor Pro (WaveMetrics) or Axograph X (Axograph).

Data were sampled at 50 kHz, filtered at 3 kHz, and then digitized by an InstruTECH ITC-18 interface (HEKA). The internal recording solution consisted of (in mM): 135 K-gluconate, 10 HEPES, 7 NaCl, 7 K2 phosphocreatine, 0.3 Na-GTP, 4 Mg-ATP (pH corrected to 7.3 with KOH). Recording electrodes were pulled from borosilicate glass and had an open tip resistance of 4-6 MΩ. Series resistance was compensated using the bridge balance circuit and was monitored throughout the experiment. Recordings in which series resistance exceeded 35 MΩ were excluded.

Prior to voltage clamp recordings, a train of action potentials was elicited using current clamp to first classify the cell as a FS, OLM, or LTH neuron. Following classification, slices were perfused with aCSF containing (in mM): 0.001 tetrodotoxin, 10 tetraethylammonium chloride, 5 4-aminopyridine, 0.1 $BaCl_2$, 0.1 $CdCl_2$, and 0.05 $NiCl_2$ to block voltage-gated sodium, potassium, and calcium channels. Voltage clamp data were acquired using an Axopatch 200B amplifier (Molecular Devices) with custom written acquisition software in Igor Pro (WaveMetrics). Neurons were held at -30 mV and inward currents were recorded in response to a series of 1000 ms hyperpolarizing voltage commands (-60 mV to -130 mV in -10 mV increments). Data were digitized at 20 kHz and filtered at 3 kHz.

**Drugs**

All drugs were obtained from Tocris, Abcam pharmaceutical, or Sigma. Drugs were prepared from a 1000x stock solution in water.

**Data analysis and statistics**

Custom written software for either Igor Pro 7 or Axograph was used to analyze all physiology data. Input resistance was calculated from the linear portion of voltage-current relationship in response to a family of 1.5 s current injections of -40 pA to 40 pA in steps of 10 pA. Action potential firing frequency was calculated from the number of action potentials during a family of 1.5 s depolarizing current steps from 0 pA to 250 pA in steps of 25 pA. All the statistical tests (unpaired t-tests, ANOVA, repeated measures of ANOVA, and Pearson's R) were performed using Prism (GraphPad)

**Immunohistochemistry**

Mice were deeply anesthetized using a ketamine/xylazine cocktail (100/10 mg/kg) and perfusion-fixed with ~20 mL of cutting saline (see above) followed by ~25 mL 4% paraformaldehyde in cutting saline at 4°C. The brain was removed, postfixed in PFA for 2 hours at RT, and placed in 30% sucrose in PBS overnight at 4°C. Horizontal thin sections (50 µm) containing the middle hippocampus were made on a cryostat (Leica) and placed in PBS. First, slices underwent antigen retrieval and were heated to between 85 °C and 95 °C for 30 minutes in 0.01M sodium citrate (pH adjusted to 6.0 with HCl) (Sigma). Slices were moved to a new plate and washed in 0.02% PBS-T 3 x 5 minutes. Slices were then incubated in a blocking buffer solution (5% normal goat serum, 0.2% triton+PBS) at RT for 1 hr, followed by primary antibodies: rabbit anti-parvalbumin (1:500, Swant) or rabbit anti-somatostatin (1:500, ImmunoStar) and mouse anti-FMRP (1:2 Developmental Studies Hybridoma Bank) in blocking solution for 48 hr at 4°C. Sections were then washed with 1x PBS 3 x 10 min and placed in blocking

solution containing secondary antibodies (1:500 488 anti-mouse, 1:500 594 anti-rabbit) and Hoerst (1:2000) for 24 hr at 4°C. The slices were washed 4 x 10 min in 1x PBS and mounted on microscope slides and cover slipped with Fluormount-g (Invitrogen).

**Imaging and Image Analysis**

The labelled sections were visualized on a Zeiss AxioImager fluorescent microscope with an ApoTome at 20x for analysis images and 40x for representative cell images. The images were captured by CCD camera, acquired by Stereo Investigator software (MBF Bioscience), and analyzed using Image J (NIH). Images were taken of the Stratum Oriens CA1 area of the hippocampus defined as the area between the CA1 pyramidal layer and the alveus and in between the subiculum and CA2/CA3. Co-expression analysis was completed in the SO CA1 using the cell counter software in Image J (NIH). Neurons were first counted and traced in the 594 channel to identify PV+ and SOM+ neurons, and then overlayed in the 488 channel to identify co-expression of FMRP.  Cells were counted if they co-expressed the interneuron marker (PV or SOM) and FMRP in stratum oriens of area CA1. Slices from 4 wild type mice across 15 sections were included in the analysis. In total, there were 171 PV and 174 SOM positive neurons that were counted for analysis, we then took the percentage of PV and SOM positive neurons that also expressed FMRP.

**Results section:**

**LTS neuron intrinsic excitability is lower in FX mice**

We made whole-cell current clamp recordings from neurons in the stratum oriens of area CA1 in the hippocampus from wild type (WT) and Fmr1 knock-out (FX) mice. After noting the resting membrane potential, neurons were held at -70 mV and two families of current injections were delivered via the recording electrode. First, a series of 1-sec long depolarizing current injections was used to measure action potential firing followed by a series of small subthreshold current injections to determine the input resistance ($R_N$). Fast spiking (FS) interneurons were identified by having a maximum action potential firing rate >100 Hz, no spike frequency adaptation, and a relatively low $R_N$ (Figure 1A-B). By contrast, low threshold spiking (LTS) interneurons were identified by having a maximum action potential firing rate <80Hz, apparent spike frequency adaptation, and a relatively high $R_N$ (Figure 1C-D).

Voltage responses to hyperpolarizing current injections in FS interneurons from both wild type and FX mice exhibited no sag or rebound and had comparatively low input resistances (<180 MΩ; Figure 2A). We found no differences in the RMP (unpaired t-test; df = 15; t=1.834; p=0.08) or $R_N$ (unpaired t-test; df = 14; t=0.065; p=0.52) between wild type and FX FS interneurons (Figure 2B-C). FS neurons exhibited the expected high frequency firing rate and no adaptation in wild type and FX mice (Figure 2D). A plot of action potentials fired as a function of current amplitude revealed no difference in the number of action potentials elicited across a range of depolarizing current amplitudes between wild type and FX FS interneurons (two-way ANOVA, main effect of genotype F(1,29)=1.107; p=0.301; Figure 2E).

In contrast to FS interneurons, subthreshold voltage responses from LTS interneurons exhibited a prominent sag and rebound in response to current injections (Figure 3A), and a comparatively high input resistance (range: 216-440 MΩ). Although there was no difference in RMP between wild type and FX LTS neurons (unpaired t-test; df = 54; t=0.69; p=0.49; Figure 3B), FX LTS neurons had a significantly lower $R_N$ compared to wild type (unpaired t-test; df = 53; t=2.622; p=0.01; Figure 3C). wild type and FX hippocampal LTS neurons exhibited the expected spike frequency adaptation (Figure 3D). When compared across a range of depolarizing current steps, FX LTS neurons fired significantly fewer action potentials compared to wild type (two-way ANOVA, main effect of genotype F(1,50)=5.69; p=0.02; Figure 3E). These data therefore suggest that the intrinsic excitability of LTS, but not FS, interneurons is lower in FX mice.

**Both FS and LTS interneurons co-express FMRP**

Given that we observed differences in both $R_N$ and action potential firing in LTS interneurons, but not FS interneurons, between wild type and FX mice, we wanted to test if there were differences in FMRP expression between FS and LTS interneurons. One of the canonical methods of identifying interneuron subtypes is the expression of specific proteins. Somatostatin (SOM) and parvalbumin (PV) are established markers of hippocampal LTS and FS interneuron subtypes respectively ((Baude et al., 2007; Tricoire et al., 2011; Chittajallu et al., 2013) but see (Hu et al., 2013; Pelkey et al., 2017)). We used immunohistochemistry to identify the coexpression of FMRP with either SOM-positive or PV-positive neurons in stratum oriens of area CA1 in wild type mice (Figure 4A-B). We found that the percentage of SOM+ (putative LTS) neurons

which co-express FMRP is greater compared to PV+ (putative FS) neurons) (unpaired t-test; df = 6; t=5.119; p=0.002; Figure 4C). Our analysis indicates SOM interneurons more reliably express FMRP compared to PV interneurons.

**LTH and OLM neurons are present in FX mice**

We recently demonstrated that LTS interneurons in stratum oriens of area of CA1 can be separated in to at least two distinct groups, oriens lacunosum-moleculare cells (OLM) and low threshold high $I_h$ cells (LTH) (Hewitt et al., 2021). One reliable measure for separating OLM and LTH cells is the degree of spike frequency adaptation (SFA). OLM neurons typically have moderate SFA and LTH neurons have more pronounced SFA. Using our previously published criteria (Hewitt et al., 2021), we separated LTS interneurons into OLM and LTH groups (Figure 5A). We found OLM and LTH neurons in roughly the same proportions between wild type and FX mice (Figure 5B). Consistent with our prior results from wild type mice, there was no correlation between interspike interval ratio (ISI), a measure of SFA, and resting membrane potential for either wild type or FX mice (Pearson's R (R Square = 0.002); Figure 5C). Spike frequency adaptation, as measured by the ISI ratio, was not different between wild type and FX mice for both LTH cells (unpaired t-test; df = 22; t=0.536; p=0.51; Figure 5D) and OLM cells (unpaired t-test; df = 30; t=0.662; p=0.59; Figure 5E).

**LTH interneurons have lower intrinsic excitability in FX mice**

We further examined recordings from OLM and LTH neurons in wild type and FX mice to compare intrinsic physiological properties. Consistent with higher $I_h$ and our previous

work (Hewitt et al., 2021), LTH interneurons have a lower $R_N$ and more prominent sag and rebound compared to OLM interneurons (Figure 6A and D). There was no difference in RMP between wild type and FX LTH neurons (Figure 6B). FX LTH neurons had a lower $R_N$ compared to wild type LTH neurons (unpaired t-test; df = 22; t=3.575; p=0.001; Figure 6C). There was no difference in RMP or $R_N$ between wild type and FX OLM interneurons (Fig. 6D-F). FX LTH interneurons fired significantly fewer action potentials compared to wild type (two-way ANOVA, main effect of genotype F(1,19)=7.971; p=0.01; Figure 7A-C). In agreement with the lack of difference in $R_N$ between wild type and FX OLM interneuron, there was no significant difference in the number of action potentials fired between wild type and FX OLM interneurons (two-way ANOVA, main effect of genotype F(1,30)=0.83; p=0.369; Figure 7 D-F).

Our results suggest that the lower input resistance in LTH neurons from FX mice accounts for the reduced action potential firing rate. During repetitive firing, the threshold for action potential firing becomes more depolarized due changes in the availability for voltage-gated sodium channels (e.g., cumulative inactivation)(Colbert and Pan, 2002). To determine if differences in action potential threshold contributed the to lower action potential firing rate in LTH neurons in FX mice, we analyzed both single (first elicited) and trains of action potentials. There was no difference in threshold for the first action potential in LTH neurons between wild type and FX mice (Figure 9A-B; unpaired- t-test, df =21, t=1.02, p= 0.31). Consistent with previous results, the threshold for action potential generation in LTH neurons depolarized across of train of 25 action potentials. There was however, no difference between wild type and FX mice (Figure

9C; two-way ANOVA, main effect of genotype F(1,16)=0.53; p=0.47). Similarly, there were no differences in threshold of the first action potential or across a train of 25 action potentials in OLM neurons between wild type and FX mice (Figure 9D-E; (unpaired t-test, df=18 t=0.28 p= 0.78); (two-way ANOVA, main effect of genotype F(1,13)=0.02, p=0.88).

**Higher $I_h$ contributes to reduced input resistance in LTH neurons from FX mice**

Both excitatory and inhibitory neurons express HCN channels ($I_h$ ) which contribute to the resting properties of the neuron (Maccaferri and McBain, 1996; Magee, 1999; Santoro et al., 2000; Lupica et al., 2001; Poolos et al., 2002). We previously showed that LTH neurons have a higher contribution of $I_h$ to the $R_N$ compared to OLM cells (Hewitt et al., 2021). To test the hypothesis that higher $I_h$ contributes to the lower $R_N$ in FX LTH neurons we made current clamp recordings from wild type and FX LTH interneurons before and after extracellular application of 50 µM ZD7288 to block HCN channels (Figure 9A). Consistent with our results in Figure 6, the baseline $R_N$ of FX LTH interneurons was significantly lower compared to wild type (unpaired t-test: t = 2.305, df = 11, p = 0.0416; Figure 9B). Given the significant contribution of $I_h$ to $R_N$ in LTH neurons, the block of $I_h$ with ZD7288 significantly increased the $R_N$ of LTH neurons in both wild type (paired t-test: t = 4.168, df = 6, p = 0.0059) and FX mice (paired t-test: t = 3.356, df = 5, p = 0.0202) (Figure 9A-B). Interestingly, $R_N$ was not significantly different between wild type and FX LTH neurons after application of ZD7288 (unpaired t-test: t = 0.3221, df = 11, p = 0.7534; Figure 9B). These results support our hypothesis that FX LTH interneurons have more $I_h$ compared to wild type.

To directly measure $I_h$ in LTH interneurons, we used a previously published voltage clamp protocol (Maccaferri and McBain, 1996; Hewitt et al., 2021). After identifying the neuron based on ISI ratio using current clamp, a cocktail of blockers was applied to isolate $I_h$ (Figure 9C). We then switched to voltage clamp and measured the current in response to a family of hyperpolarizing voltage steps from a holding potential of -30 mV before and after application of the HCN channel blocker ZD7288 (50 µM). Subtraction of the current after ZD7288 from the baseline current isolated the ZD sensitive current, $I_h$. Consistent with the prominent sag and rebound, a slowly activating ZD-sensitive inward current was recorded from both wild type and FX LTH interneurons (Figure 9D-E). In agreement with our hypothesis, we found that the ZD-sensitive current was larger in LTH interneurons from FX mice compared to wild type (two-way ANOVA, main effect of genotype: $F(1,29)=1.107$, $p=0.0005$; Figure 9F-G).

## Discussion

A disruption of the balance between excitation and inhibition is one working hypothesis that may explain some of the neuropathology of FXS. Although there are many studies investigating excitatory pyramidal neurons in FXS, investigations of inhibitory interneurons are lacking. We investigated the intrinsic physiological properties of FS and LTS inhibitory interneurons in the stratum oriens of area CA1 in the hippocampus from wild type and FX mice. We found no differences in either subthreshold properties or action potential firing between wild type and FX FS interneurons. By contrast, FX LTS interneurons had a lower input resistance and fired fewer action potentials compared to

wild type. We used the interneuron markers parvalbumin (PV) to label putative fast spiking interneurons and somatostatin (SOM) to label putative low threshold spiking interneurons and determine the co-expression of FMRP. Although both PV+ and SOM+ cells expressed FMRP, SOM+ neurons more reliably expressed FMRP compared to PV+ cells. As described in our recent paper (Hewitt et al., 2021), we subdivided low threshold spiking interneurons into OLM and LTH interneurons. Current clamp experiments revealed FX LTH, but not OLM, interneurons had a significantly lower input resistance and fired fewer action potentials across a family of current steps. Current clamp and voltage clamp experiments showed that FX LTH neurons were more sensitive to the h-channel blocker ZD7288 suggesting that the differences in intrinsic properties we due in part to higher $I_h$.

Changes in voltage-gated ion channel function and expression, including HCN channels, were identified in FX excitatory pyramidal cells (Brager et al., 2012; Deng et al., 2013, 2019; Zhang et al., 2014; Kalmbach et al., 2015; Deng and Klyachko, 2016; Routh et al., 2017). Here we show FX LTH interneurons have a lower input resistance due in part to a larger h-channel current. While we do not observe the typical depolarization of the RMP this could be due in part to differences in either the kinetics of h-channels in FX LTH neurons or the localization (dendritic vs somatic expression) of h-channels in the cell. To gain insight in to these two potential mechanisms an experimental paradigm that would address space clamp limitations, such as outside-out voltage clamp recordings, would be required to properly determine h-channel kinetics. Outside-out voltage clamp along the somato-dendritic axis would be ideal to determine the h-channel current at specific anatomical regions of LTH neurons. An enrichment of

HCN channels in the dendrites of FX LTH neurons would not influence the RMP as drastically as somatic expression of HCN, therefore; it is possible that FX LTH neurons to have more h-channel expression in the dendrites compared to WT LTH neurons. Additionally, m-type channels can also contribute to the input resistance of neurons (Lawrence et al., 2006). It could be the case, and indeed probable, that multiple ion channels are contributing to the altered intrinsic excitability of LTH neurons in FX mice.

Previously published reports found changes in FS interneurons in FX mice. In primary visual cortex, spatial selectivity of cortical FS PV-positive interneurons is decreased in FX mice (Goel et al., 2018). In layer 4 of somatosensory cortex, FS neurons in FX mice have higher input resistance and action potential firing rate compared to wild type mice (Domanski et al., 2019). Given our previous work showing that changes in HCN channels in FX mice occurs in a brain region specific manner (Brager et al., 2012; Kalmbach et al., 2015; Brandalise et al., 2020), perhaps is not too surprising that the loss of FMRP has differential effects on FS neurons in the cortex and hippocampus. While we saw no difference in intrinsic properties of FS neurons between wild type and FX mice, changes in the excitatory synaptic drive onto FS neurons or the inhibitory synaptic drive onto downstream neurons may be different in FX mice.

**Inhibitory deficits in Fragile X syndrome**

There are many types of inhibitory interneurons in the hippocampus that gate activity flow, influence synaptic plasticity, and exhibit control over rhythmic activity (Cobb et al., 1995; Klausberger et al., 2003; Gloveli et al., 2005; Lovett-Barron et al., 2014; Adler et al., 2019). Fast spiking interneurons (FS) make up roughly 14% of the CA1 interneuron

population and are located near the pyramidal cell layer or in the stratum oriens where many exhibit strong inhibition on the cell body of pyramidal cells (Bezaire and Soltesz, 2013). FS interneurons in area CA1 provide strong feedforward inhibition as they receive excitatory input from many CA3 pyramidal cells (Buhl et al., 1994; Sik et al., 1995). Low threshold spiking interneurons (LTS) account for approximately 4.5% of total CA1 interneurons and predominantly target the distal dendrites of pyramidal cells in SLM (Bezaire and Soltesz, 2013). LTS interneurons in area CA1 form a canonical feedback inhibition circuit and receive most of their excitatory input from CA1 pyramidal cells (Ali et al., 1998; Klausberger, 2009).

Together FS and LTS inhibitory interneurons play a critical role in balancing excitatory activity (Klausberger and Somogyi, 2008; Pelkey et al., 2017). Proper inhibitory signaling promotes intact plasticity and guides network wide oscillatory events that are critical for learning and memory (Freund and Buzsáki, 1996; Jinno et al., 2007). Several studies on cortical inhibition in FX mice highlighted changes in both FS and LTS interneurons (Gibson et al., 2008; Goel et al., 2018; Domanski et al., 2019). Reduced activation of LTS neurons by metabotropic glutamate receptor signaling and decreased synchronization in synaptic inhibition suggest weakened LTS signaling in somatosensory cortex (Paluszkiewicz et al., 2011a). Network hyperexcitability, measured as prolong UP states, in somatosensory cortex is due in part to decreased inhibitory activity from FS neurons (Gibson et al., 2008). These studies demonstrate the importance of investigating specific types of inhibitory interneurons to understand how changes in inhibition contribute to FX pathology.

Although there are several known hippocampal functions that require appropriate stratum oriens inhibitory interneuron signaling (Lovett-Barron et al., 2014; Adler et al., 2019), there are surprisingly few investigations that directly investigate the hippocampal inhibitory interneurons of this region in FX models. We found that LTH neurons in FX mice were less excitable compared to wild type mice. While the location of the axon and synaptic contacts of CA1 LTH neurons remains unknown, the reduced action potential firing would lead to reduced inhibitory drive of hippocampal circuits. If like OLM neurons, LTH neurons provide feedback inhibition onto CA1 pyramidal neurons, the reduced excitability of FX LTH neurons would make the synaptic excitation from CA1 neurons less effective, thus reducing feedback inhibition. While we did not measure synaptic inhibition in this study, other studies reported reduced inhibitory drive onto pyramidal cells in CA1 in the FX hippocampus (Wahlstrom-Helgren and Klyachko, 2015; Sabanov et al., 2017). It is unclear in either of these studies however, which type of inhibitory interneuron(s) were the source of this inhibition. Additionally, a reduction in inhibitory drive from decreased intrinsic excitability from FX LTH neurons could result in poor modulation of CA1 neuron output. FX mice have been shown to exhibit unstable theta-gamma coupling in the CA1 hippocampus ((Talbot et al., 2018). This discoordination of hippocampal rhythms could be a result of decreased LTH neuron output, and therefore unreliable control, of CA1 pyramidal neuron activity.

FXS patients display several behavioral deficits associated with hippocampal dysfunction such as epilepsy and sensory hypersensitivity. One of the leading hypotheses of these behavioral deficits in FXS is an imbalance of excitatory/inhibitory activity in the hippocampus. Each inhibitory interneuron subtype plays a specific role in

orchestrating the flow of excitatory activity through the hippocampus and a deficit in even one subtype in FXS could contribute to hippocampal dysfunction. We found that LTH inhibitory interneurons, a recently identified subclass of low threshold spiking neurons, in the CA1 stratum oriens of the hippocampus in FX mice have higher expression of the hyperpolarization activated cation current, $I_h$. The higher $I_h$ in FX LTH neurons contributed lower input resistance and reduced action potential firing rate compared to WT LTH neurons. These changes contribute to lower intrinsic excitability of CA1 stratum oriens LTH neurons in FX mice, which can potentially alter the E/I balance of the CA1 hippocampal circuit. This study highlights the importance of investigating hippocampal interneurons in a subtype and brain region specific fashion which is critical to understanding the cellular basis for neurological deficits in FXS.

**Acknowledgements:** We thank Kim Pantagma for the processing of the hippocampal immunohistochemistry, members of the Johnston and Brager lab for helpful comments and lively discussion of this manuscript, and Dr. Richard Gray for essential assistance with analysis and acquisition software. This work was supported by the Nation Institutes of Health grant RO1 MH100510 (DHB), the National Foundation of Sciences GRFP (LTH), and The University of Texas at Austin continuing graduate student fellowship (LTH).

**Author Contributions:** L.T.H. and D.H.B. designed experiments; L.T.H. and D.H.B. acquired data; L.T.H. and D.H.B. analyzed data; L.T.H. and D.H.B. interpreted results of

experiments; L.T.H. and D.H.B. prepared figures; L.T.H. and D.H.B. drafted manuscript; L.T.H. and D.H.B. edited and revised manuscript.

**Disclosures:** The authors declare no conflicts of interest

**Dedication:** This manuscript is dedicated to Dr. Richard Gray, our instrumental colleague whose legacy has made a lasting impact to the field of hippocampal neurophysiology.

## References:


1. Adler A, Zhao R, Shin ME, Yasuda R, Gan W-B (2019) Somatostatin-Expressing Interneurons Enable and Maintain Learning-Dependent Sequential Activation of Pyramidal Neurons. Neuron 102:202-216.e7.

2. Ali AB, Deuchars J, Pawelzik H, Thomson AM (1998) CA1 pyramidal to basket and bistratified cell EPSPs: dual intracellular recordings in rat hippocampal slices. J Physiol 507 ( Pt 1):201–217.

3. Baude A, Bleasdale C, Dalezios Y, Somogyi P, Klausberger T (2007) Immunoreactivity for the GABAA Receptor 1 Subunit, Somatostatin and Connexin36 Distinguishes Axoaxonic, Basket, and Bistratified Interneurons of the Rat Hippocampus. Cerebral Cortex 17:2094–2107.

4. Bell MV, Hirst MC, Nakahori Y, MacKinnon RN, Roche A, Flint TJ, Jacobs PA, Tommerup N, Tranebjaerg L, Froster-Iskenius U, Kerr B, Turner G, Lindenbaum RH, Winter R, Prembrey M, Thibodeau S, Davies KE (1991) Physical mapping across the fragile X: Hypermethylation and clinical expression of the fragile X syndrome. Cell 64:861–866.

5. Belmonte MK, Bourgeron T (2006) Fragile X syndrome and autism at the intersection of genetic and neural networks. Nat Neurosci 9:1221–1225.

6. Bezaire MJ, Soltesz I (2013) Quantitative Assessment of CA1 Local Circuits: Knowledge Base for Interneuron-Pyramidal Cell Connectivity. Hippocampus 23:751–785.

7. Brager DH, Akhavan AR, Johnston D (2012) Impaired Dendritic Expression and Plasticity of h-Channels in the fmr1−/y Mouse Model of Fragile X Syndrome. Cell Reports 1:225–233.

8. Brandalise F, Kalmbach BE, Mehta P, Thornton O, Johnston D, Zemelman BV, Brager DH (2020) Fragile X Mental Retardation Protein Bidirectionally Controls Dendritic $I_h$ in a Cell Type-Specific Manner between Mouse Hippocampus and Prefrontal Cortex. J Neurosci 40:5327–5340.

9. Buhl EH, Halasy K, Somogyi P (1994) Diverse sources of hippocampal unitary inhibitory postsynaptic potentials and the number of synaptic release sites. Nature 368:823–828.

10. Chao H-T, Chen H, Samaco RC, Xue M, Chahrour M, Yoo J, Neul JL, Gong S, Lu H-C, Heintz N, Ekker M, Rubenstein JLR, Noebels JL, Rosenmund C, Zoghbi HY (2010) Dysfunction in GABA signalling mediates autism-like stereotypies and Rett syndrome phenotypes. Nature 468:263–269.

11. Chittajallu R, Craig MT, McFarland A, Yuan X, Gerfen S, Tricoire L, Erkkila B, Barron SC, Lopez CM, Liang BJ, Jeffries BW, Pelkey KA, McBain CJ (2013) Dual origins of functionally

distinct O-LM interneurons revealed by differential 5-$HT_{3A}$R expression. Nature Neuroscience 16:1598–1607.

12. Cobb SR, Buhl EH, Halasy K, Paulsen O, Somogyi P (1995) Synchronization of neuronal activity in hippocampus by individual GABAergic interneurons. Nature 378:75–78.

13. Colbert CM, Pan E (2002) Ion channel properties underlying axonal action potential initiation in pyramidal neurons. Nat Neurosci 5:533–538.

14. Contractor A, Klyachko VA, Portera-Cailliau C (2015) Altered neuronal and circuit excitability in Fragile X Syndrome. Neuron 87:699–715.

15. DeFelipe J et al. (2013) New insights into the classification and nomenclature of cortical GABAergic interneurons. Nat Rev Neurosci 14:202–216.

16. Deng P-Y, Carlin D, Oh YM, Myrick LK, Warren ST, Cavalli V, Klyachko VA (2019) Voltage-Independent SK-Channel Dysfunction Causes Neuronal Hyperexcitability in the Hippocampus of Fmr1 Knock-Out Mice. J Neurosci 39:28–43.

17. Deng P-Y, Klyachko VA (2016) Genetic upregulation of BK channel activity normalizes multiple synaptic and circuit defects in a mouse model of fragile X syndrome. The Journal of Physiology 594:83–97.

18. Deng P-Y, Rotman Z, Blundon JA, Cho Y, Cui J, Cavalli V, Zakharenko SS, Klyachko VA (2013) FMRP Regulates Neurotransmitter Release and Synaptic Information Transmission by Modulating Action Potential Duration via BK Channels. Neuron 77:696–711.

19. Domanski APF, Booker SA, Wyllie DJA, Isaac JTR, Kind PC (2019) Cellular and synaptic phenotypes lead to disrupted information processing in Fmr1-KO mouse layer 4 barrel cortex. Nat Commun 10:4814.

20. Feng Y, Gutekunst CA, Eberhart DE, Yi H, Warren ST, Hersch SM (1997) Fragile X mental retardation protein: nucleocytoplasmic shuttling and association with somatodendritic ribosomes. J Neurosci 17:1539–1547.

21. Freund TF, Buzsáki G (1996) Interneurons of the hippocampus. Hippocampus 6:347–470.

22. Fu Y-H, Kuhl DPA, Pizzuti A, Pieretti M, Sutcliffe JS, Richards S, Verkert AJMH, Holden JJA, Fenwick RG, Warren ST, Oostra BA, Nelson DL, Caskey CT (1991) Variation of the CGG repeat at the fragile X site results in genetic instability: Resolution of the Sherman paradox. Cell 67:1047–1058.

23. Gibson JR, Bartley AF, Hays SA, Huber KM (2008) Imbalance of Neocortical Excitation and Inhibition and Altered UP States Reflect Network Hyperexcitability in the Mouse Model of Fragile X Syndrome. Journal of Neurophysiology 100:2615–2626.

24. Gloveli T, Dugladze T, Saha S, Monyer H, Heinemann U, Traub RD, Whittington MA, Buhl EH (2005) Differential involvement of oriens/pyramidale interneurones in hippocampal network oscillations in vitro. The Journal of Physiology 562:131–147.

25. Goel A, Cantu DA, Guilfoyle J, Chaudhari GR, Newadkar A, Todisco B, de Alba D, Kourdougli N, Schmitt LM, Pedapati E, Erickson CA, Portera-Cailliau C (2018) Impaired perceptual learning in a mouse model of Fragile X syndrome is mediated by parvalbumin neuron dysfunction and is reversible. Nat Neurosci 21:1404–1411.

26. Hagerman RJ, Berry-Kravis E, Kaufmann WE, Ono MY, Tartaglia N, Lachiewicz A, Kronk R, Delahunty C, Hessl D, Visootsak J, Picker J, Gane L, Tranfaglia M (2009) Advances in the Treatment of Fragile X Syndrome. Pediatrics 123:378–390.

27. Hagerman RJ, Hagerman PJ (2002) The fragile X premutation: into the phenotypic fold. Current Opinion in Genetics & Development 12:278–283.

28. Hall SS, Lightbody AA, Reiss AL (2008) Compulsive, self-injurious, and autistic behavior in children and adolescents with fragile X syndrome. Am J Ment Retard 113:44–53.

29. Hewitt LT, Ordemann GJ, Brager DH (2021) High and low expression of the hyperpolarization activated current (Ih) in mouse CA1 stratum oriens interneurons. Physiological Reports 9:e14848.

30. Hu H, Cavendish JZ, Agmon A (2013) Not all that glitters is gold: off-target recombination in the somatostatin–IRES-Cre mouse line labels a subset of fast-spiking interneurons. Front Neural Circuits 7 Available at: https://www.frontiersin.org/articles/10.3389/fncir.2013.00195/full [Accessed February 25, 2021].

31. Jinno S, Klausberger T, Marton LF, Dalezios Y, Roberts JDB, Fuentealba P, Bushong EA, Henze D, Buzsáki G, Somogyi P (2007) Neuronal Diversity in GABAergic Long-Range Projections from the Hippocampus. J Neurosci 27:8790–8804.

32. Kalmbach BE, Johnston D, Brager DH (2015) Cell-Type Specific Channelopathies in the Prefrontal Cortex of the fmr1-/y Mouse Model of Fragile X Syndrome. eNeuro 2 Available at: https://www.eneuro.org/content/2/6/eneuro.0114-15.2015 [Accessed May 17, 2020].

33. Kaufmann WE, Cortell R, Kau ASM, Bukelis I, Tierney E, Gray RM, Cox C, Capone GT, Stanard P (2004) Autism spectrum disorder in fragile X syndrome: Communication, social interaction, and specific behaviors. American Journal of Medical Genetics Part A 129A:225–234.

34. Klausberger T (2009) GABAergic interneurons targeting dendrites of pyramidal cells in the CA1 area of the hippocampus. European Journal of Neuroscience 30:947–957.

35. Klausberger T, Magill PJ, Márton LF, Roberts JDB, Cobden PM, Buzsáki G, Somogyi P (2003) Brain-state- and cell-type-specific firing of hippocampal interneurons in vivo. Nature 421:844–848.

36. Klausberger T, Somogyi P (2008) Neuronal Diversity and Temporal Dynamics: The Unity of Hippocampal Circuit Operations. Science 321:53–57.

37. Lawrence JJ, Saraga F, Churchill JF, Statland JM, Travis KE, Skinner FK, McBain CJ (2006) Somatodendritic Kv7/KCNQ/M Channels Control Interspike Interval in Hippocampal Interneurons. J Neurosci 26:12325–12338.

38. Lovett-Barron M, Kaifosh P, Kheirbek MA, Danielson N, Zaremba JD, Reardon TR, Turi GF, Hen R, Zemelman BV, Losonczy A (2014) Dendritic Inhibition in the Hippocampus Supports Fear Learning. Science 343:857–863.

39. Lupica CR, Bell JA, Hoffman AF, Watson PL (2001) Contribution of the Hyperpolarization-Activated Current ( $I_h$ ) to Membrane Potential and GABA Release in Hippocampal Interneurons. Journal of Neurophysiology 86:261–268.

40. Maccaferri G, McBain CJ (1996) The hyperpolarization-activated current (Ih) and its contribution to pacemaker activity in rat CAI hippocampal stratum oriens-alveus interneurones. J Physiol:12.

41. Magee JC (1999) Dendritic Ih normalizes temporal summation in hippocampal CA1 neurons. Nat Neurosci 2:508–514.

42. Paluszkiewicz SM, Martin BS, Huntsman MM (2011a) Fragile X Syndrome: The GABAergic System and Circuit Dysfunction. DNE 33:349–364.

43. Paluszkiewicz SM, Olmos-Serrano JL, Corbin JG, Huntsman MM (2011b) Impaired inhibitory control of cortical synchronization in fragile X syndrome. Journal of Neurophysiology 106:2264–2272.

44. Pelkey KA, Chittajallu R, Craig MT, Tricoire L, Wester JC, McBain CJ (2017) Hippocampal GABAergic Inhibitory Interneurons. Physiological Reviews 97:1619–1747.

45. Poolos NP, Migliore M, Johnston D (2002) Pharmacological upregulation of h-channels reduces the excitability of pyramidal neuron dendrites. Nat Neurosci 5:767–774.

46. Routh BN, Johnston D, Brager DH (2013) Loss of Functional A-Type Potassium Channels in the Dendrites of CA1 Pyramidal Neurons from a Mouse Model of Fragile X Syndrome. J Neurosci 33:19442–19450.

47. Routh BN, Rathour RK, Baumgardner ME, Kalmbach BE, Johnston D, Brager DH (2017) Increased transient Na+ conductance and action potential output in layer 2/3 prefrontal cortex neurons of the fmr1−/y mouse. J Physiol 595:4431–4448.

48. Rubenstein JLR, Merzenich MM (2003) Model of autism: increased ratio of excitation/inhibition in key neural systems. Genes Brain Behav 2:255–267.

49. Sabanov V, Braat S, D'Andrea L, Willemsen R, Zeidler S, Rooms L, Bagni C, Kooy RF, Balschun D (2017) Impaired GABAergic inhibition in the hippocampus of Fmr1 knockout mice. Neuropharmacology 116:71–81.

50. Santoro B, Chen S, Lüthi A, Pavlidis P, Shumyatsky GP, Tibbs GR, Siegelbaum SA (2000) Molecular and Functional Heterogeneity of Hyperpolarization-Activated Pacemaker Channels in the Mouse CNS. J Neurosci 20:5264–5275.

51. Sik A, Penttonen M, Ylinen A, Buzsaki G (1995) Hippocampal CA1 interneurons: an in vivo intracellular labeling study. J Neurosci 15:6651–6665.

52. Talbot ZN, Sparks FT, Dvorak D, Curran BM, Alarcon JM, Fenton AA (2018) Normal CA1 Place Fields but Discoordinated Network Discharge in a Fmr1-Null Mouse Model of Fragile X Syndrome. Neuron 97:684-697.e4.

53. Tricoire L, Pelkey KA, Erkkila BE, Jeffries BW, Yuan X, McBain CJ (2011) A Blueprint for the Spatiotemporal Origins of Mouse Hippocampal Interneuron Diversity. J Neurosci 31:10948–10970.

54. Wahlstrom-Helgren S, Klyachko VA (2015) GABAB receptor-mediated feed-forward circuit dysfunction in the mouse model of fragile X syndrome. J Physiol 593:5009–5024.

55. Zhang Y, Bonnan A, Bony G, Ferezou I, Pietropaolo S, Ginger M, Sans N, Rossier J, Oostra B, LeMasson G, Frick A (2014) Dendritic channelopathies contribute to neocortical and sensory hyperexcitability in Fmr1−/y mice. Nat Neurosci 17:1701–1709.

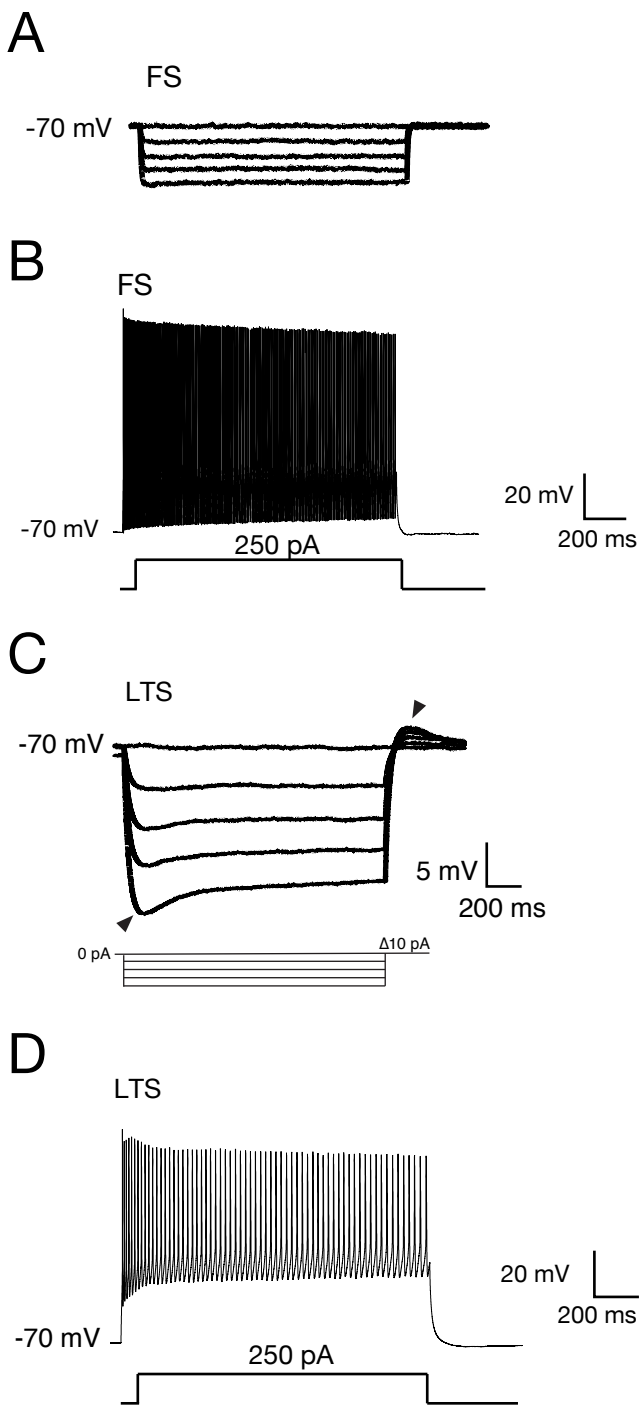


**Figure 1: Physiological identification of fast spiking and low-threshold spiking interneuron subtypes**

a) Voltage traces of a FS interneuron to a series of subthreshold steps, note the lack of sag and rebound. b) Voltage traces of a FS interneuron to a 1500 ms 250 pA current step, note the high firing rate (>100 Hz) and lack of adaptation. c) voltage traces of a LTS neuron to a series of hyperpolarizing voltage steps, note the sag and rebound responses. d) Voltage traces of a LTS neuron to a 1500 ms 250 pA step, note the spike adaptation.

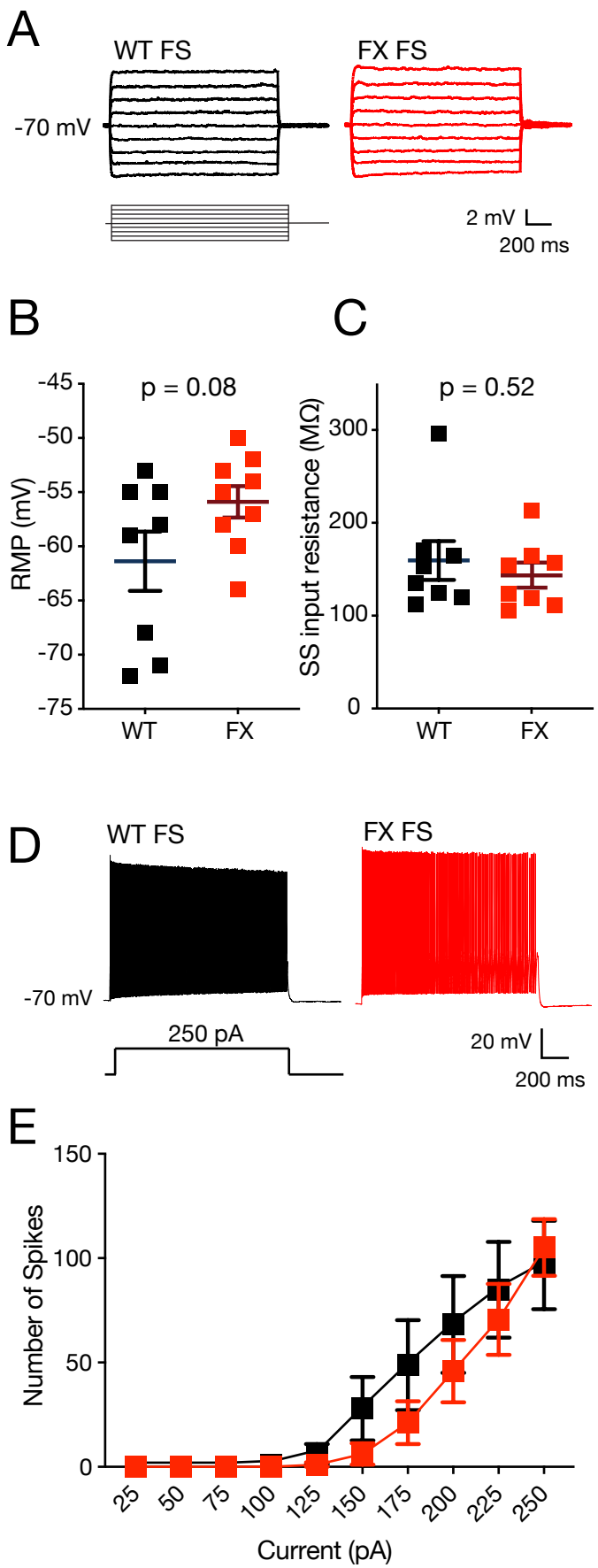


**Figure 2: Fast spiking stratum oriens neurons are not different between WT and FX mice**

a) Voltage traces showing the response to a family of current steps in WT and FX FS neurons. b) No differences in resting membrane potential between WT and FX FS cells (unpaired t-test; df = 15; t=1.834; p=0.08) c) No difference in the steady state input resistance of WT and FX FS cells (unpaired t-test; df = 14; t=0.065; p=0.52) d) Action potential voltage traces of FS neurons in response to 250 pA step of current. e) the number of spikes elicited by a family of current steps is not different between WT and FX neurons (two-way ANOVA, main effect of genotype F(1,29)=1.107; p=0.301).

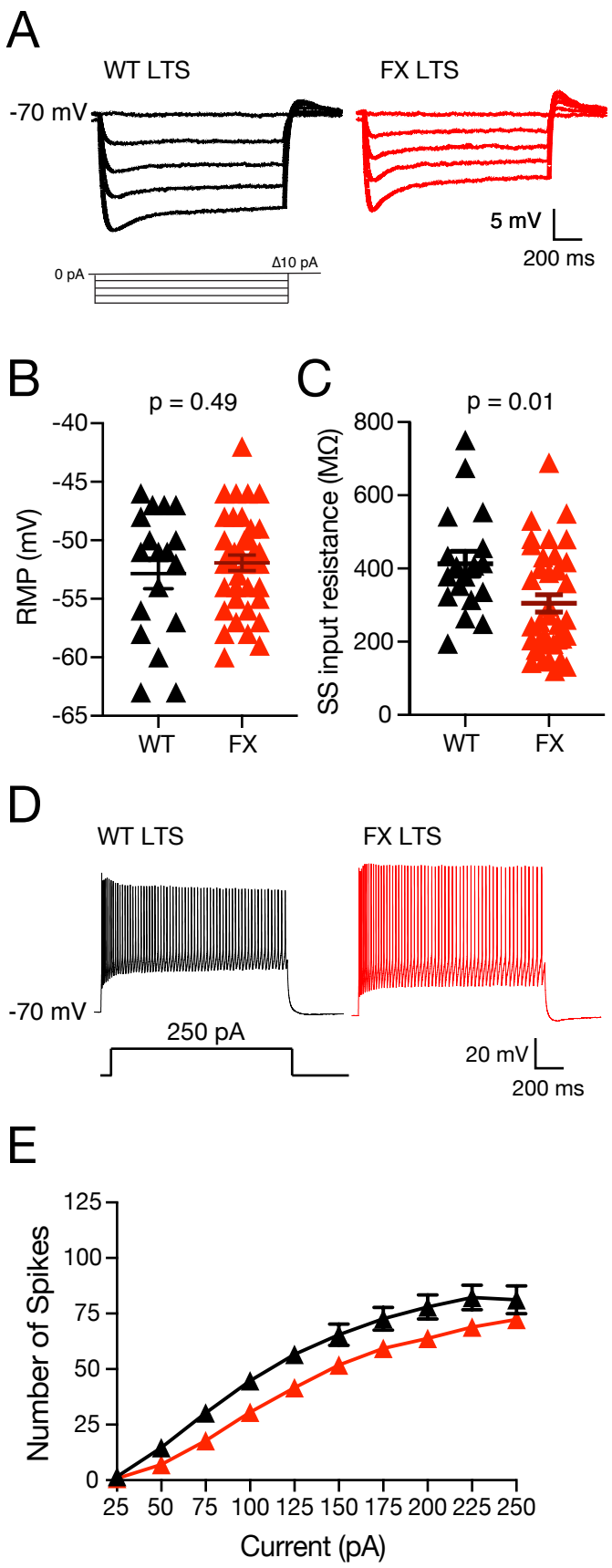


**Figure 3: Both subthreshold and suprathreshold properties of low-threhsold stratum oriens neurons are altered in FX mice compared to WT**

a) Voltage traces of WT and FX LTS cells in response to a family of hyperpolarizing current steps. b) No difference in the resting membrane potential between WT and FX LTS neurons (unpaired t-test; df = 54; t=0.69; p=0.49). c) FX LTS neurons have a lower input resistance than WT LTS neurons (unpaired t-test; df = 53; t=2.622; p=0.01) d) voltage deflections of WT and FX LTS neurons in response to a 250 pA current step. e) FX LTS neurons have fewer APs in response to a family of depolarizing current steps (repeated measures ANOVA, main effect of genotype (F (1,50) = 5.69; p = 0.02)).

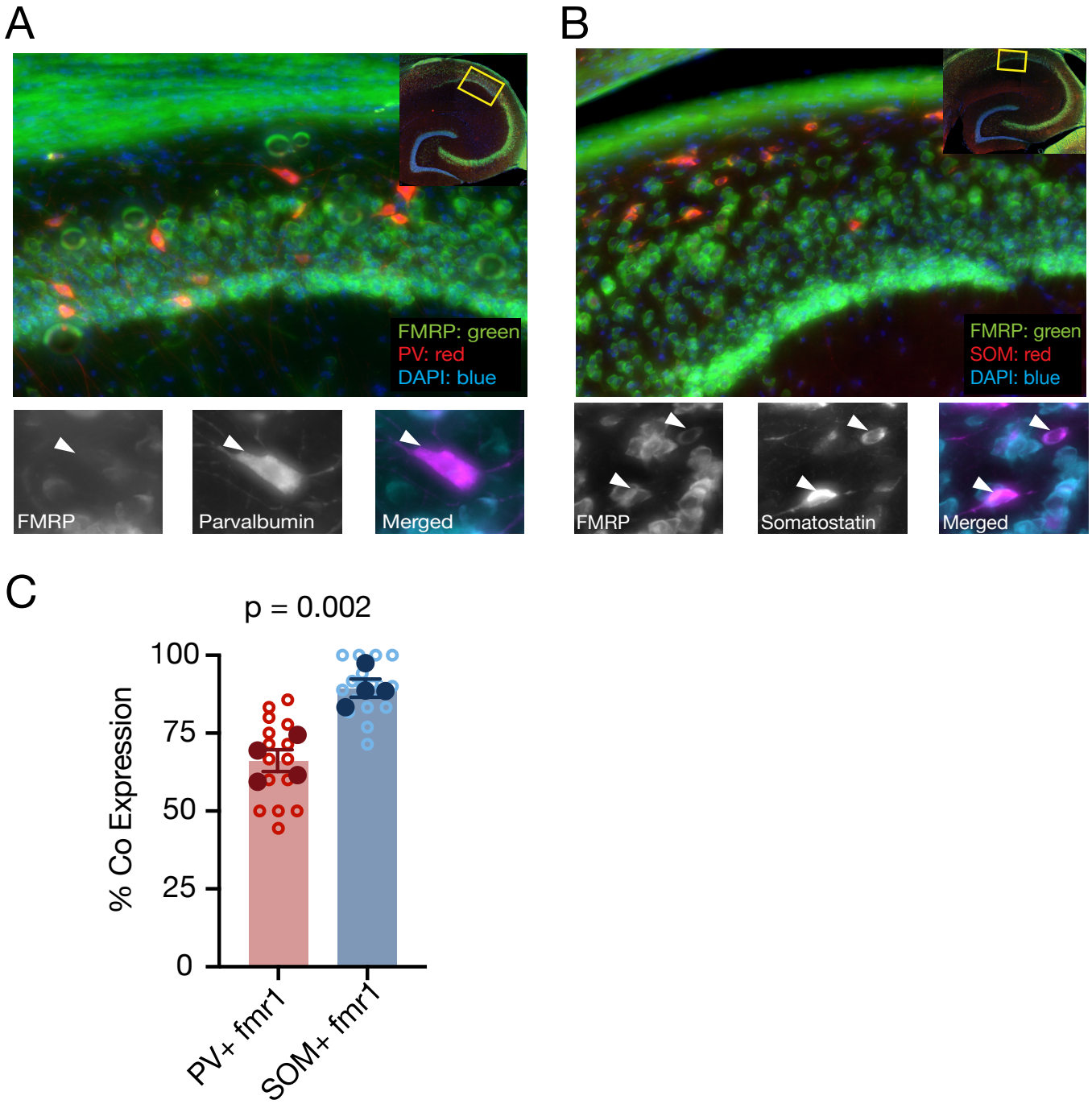


**Figure 4: Immunohistochemistry analysis of FMRP co-expression with PV and SOM**

a) High resolution image of CA1 region shown in inset. FMRP expression in green, PV expression in red, and DAPI in blue. Individual PV+ cell image shown below in 40x magnification with FMRP expression, PV expression, and the merged images. b) High resolution image of the CA1 region shown in inset. FMRP expression in green, SOM in red, and DAPI in blue. Individual SOM+ cell image in 40x shown below with FMRP expression, SOM expression, and the merged images. c) Percent co-expression (interneuron marker / FMRP+ neurons) of FMRP in PV+ and SOM+ neurons, CA1 SOM+ neurons show more co-expression with FMRP compared to CA1 PV+ neurons (n=4, unpaired t-test; df = 6; t=5.119; p=0.002).

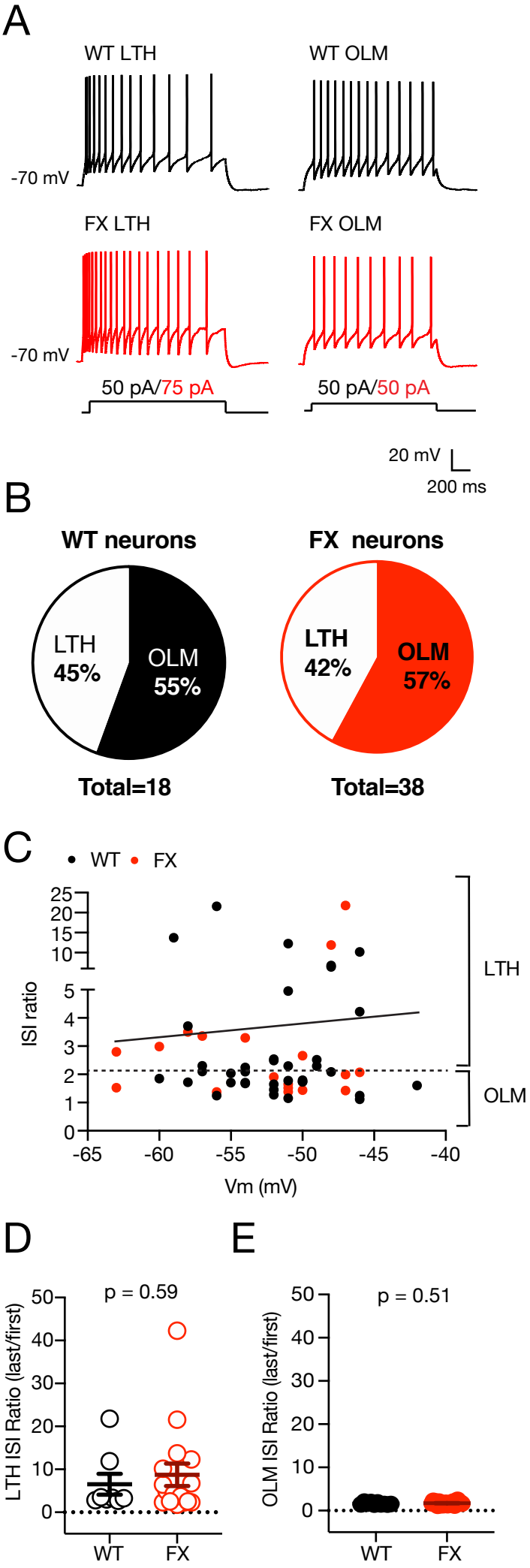


**Figure 5: Separation of low threshold spiking cells into two separate cell types: OLM and LTH in the FX hippocampus**

a) Voltage traces of WT LTH and OLM neurons in black and FX LTH and OLM neurons in red. Voltage traces represent the first current step to elicit action potentials (75 pA and 50 pA respectively). b) Solid line indicates the linear regression of LTH and OLM cells ISI ratio vs RMP (Pearson's R (R Square = 0.002)) Dashed line indicates the ISI ratio cut off between LTH and OLM neurons. c) No differences between WT and FX ISI ratio in LTH neurons (unpaired t-test; df = 22; t=0.536; p=0.51). d) No differences between WT and FX ISI ratio in OLM neurons (unpaired t-test; df = 30; t=0.662; p=0.59).

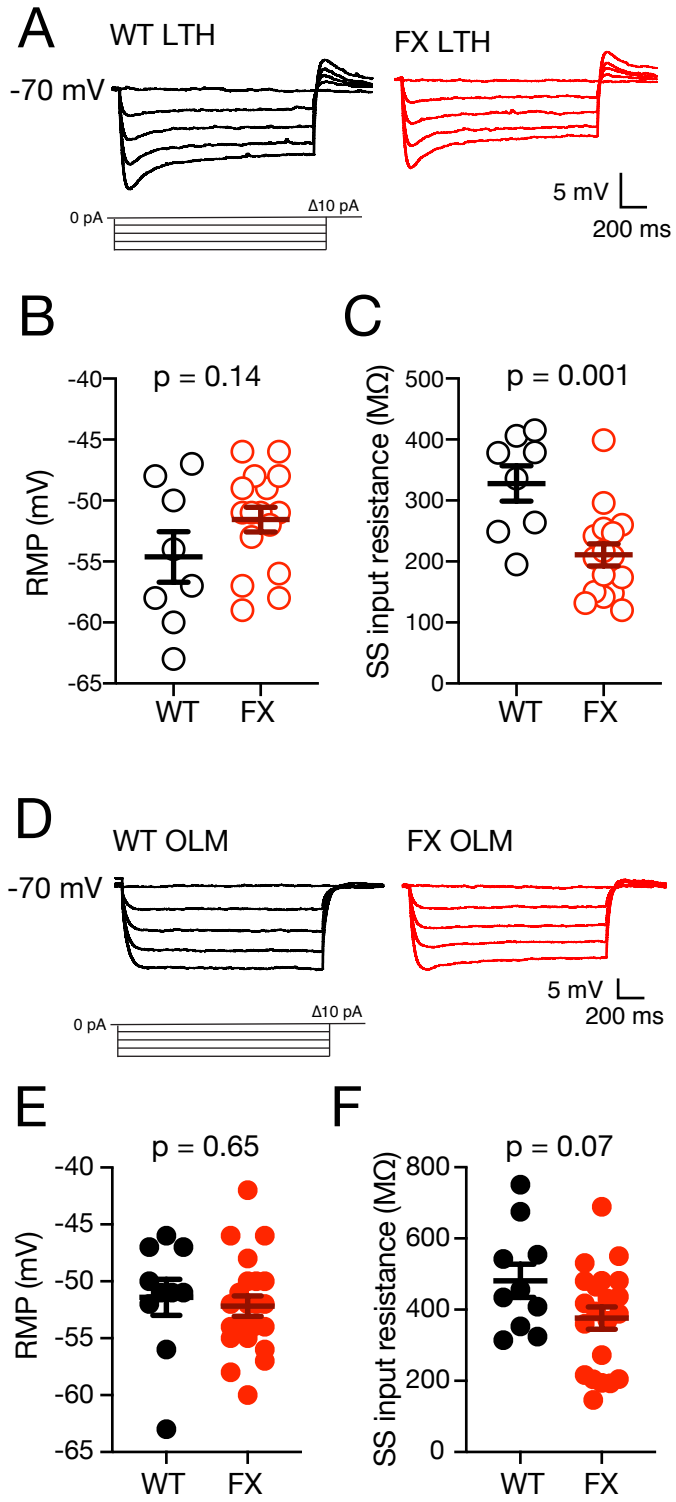


**Figure 6: LTH, but not OLM, neurons have a lower input resistance in the FX hippocampus compared to WT**

a) Voltage traces of CA1 LTH WT and FX LTH neurons in response to family of hyper polarizing current steps. b) no significant differences in resting membrane potential between WT and FX LTH cells (unpaired t-test, p = 0.14). c) FX LTH neurons show a lower input resistance compared to WT LTH neurons (unpaired t-test; df = 22; t=3.575; p=0.001). d) Voltage traces of WT and FX OLM neurons in response to a family of hyperpolarizing current steps. e) no differences in the resting membrane potential of WT and FX OLM neurons (unpaired t-test, p = 0.65). f) no differences in steady-state input resistance of WT and FX OLM cells (unpaired t-test, p = 0.07).

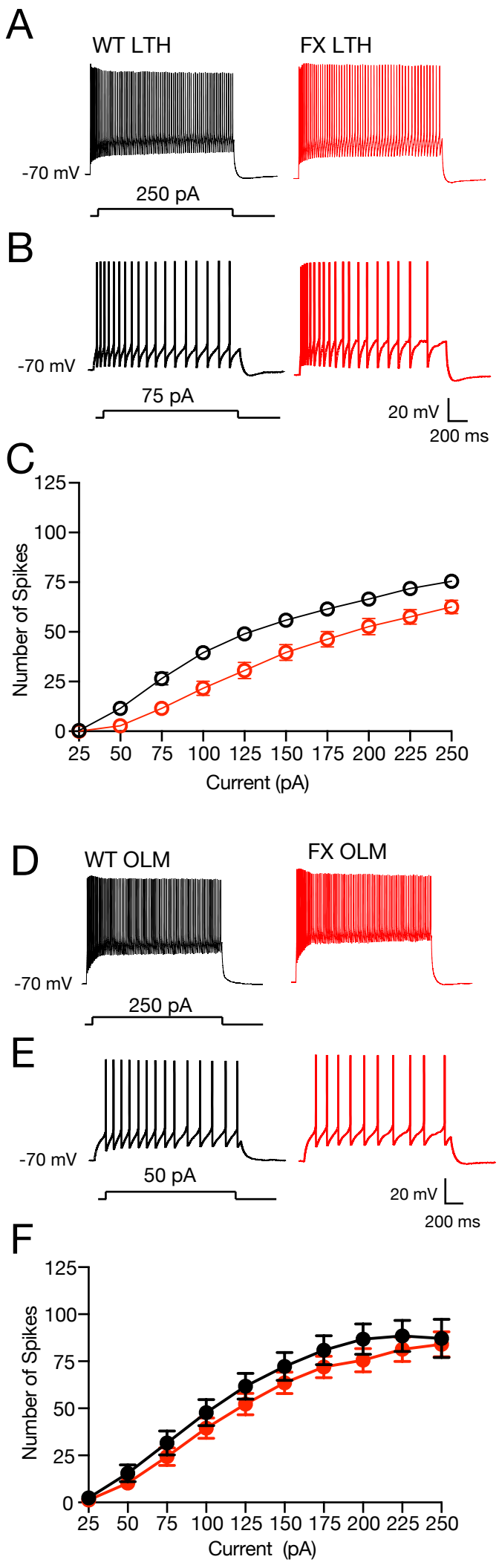


**Figure 7: FX LTH, but not FX OLM, neurons fire significantly less APs compared to WT**

a) Voltage traces of WT and FX LTH neurons in response to a 250 pA current step b) The first current step to elicit spikes in WT and FX neurons: 75 pA. c) graph of the number of spikes elicited to a family of depolarizing current injections. FX LTH neurons fired significantly less APs compared to WT LTH neurons (repeated measures ANOVA, main effect of current ($F(1.24,21.26)=262.5$; $p = 0.0001$), main effect of genotype ($F(1,19) = 7.971$; $p = 0.01$), interaction between current and genotype ($F(9,171)=3.14$; $p = 0.001$). d) Voltage traces of WT and FX OLM interneurons in response to a 250 pA step. e) Voltage traces of WT and FX OLM neurons for the first current step to elicit APs, 50 pA f) No significant differences in the number of APs fired in response to a family of depolarizing current steps in WT and FX OLM interneurons.

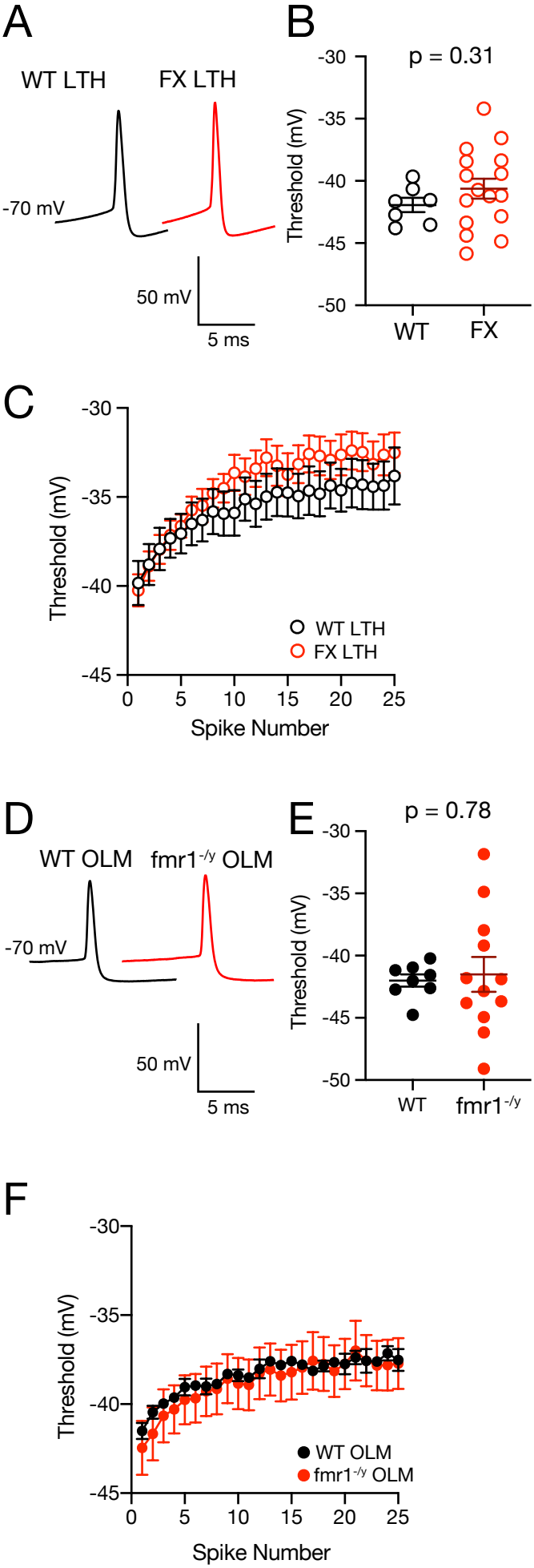


**Figure 8: Action potential threshold in LTH and OLM neurons is not different between WT and FX mice**

a) Traces of the first action potential from WT and FX LTH neurons. b) No difference in AP threshold between WT and FX LTH neurons (unpaired- t-test, df =21, t=1.02, p= 0.31). c) No difference in threshold across a train of 25 action potentials between WT and FX LTH neurons (two-way ANOVA, main effect of genotype F(1,16)=0.53; p=0.47). d) Traces of the first action potential from WT and FX OLM neurons. e) No difference in threshold between WT and FX OLM cells (unpaired t-test, df=18 t=0.28 p= 0.78) f) No difference in threshold across a train of 25 action potentials between WT and FX OLM neurons (two-way ANOVA, main effect of genotype F(1,13)=0.02, p=0.88).

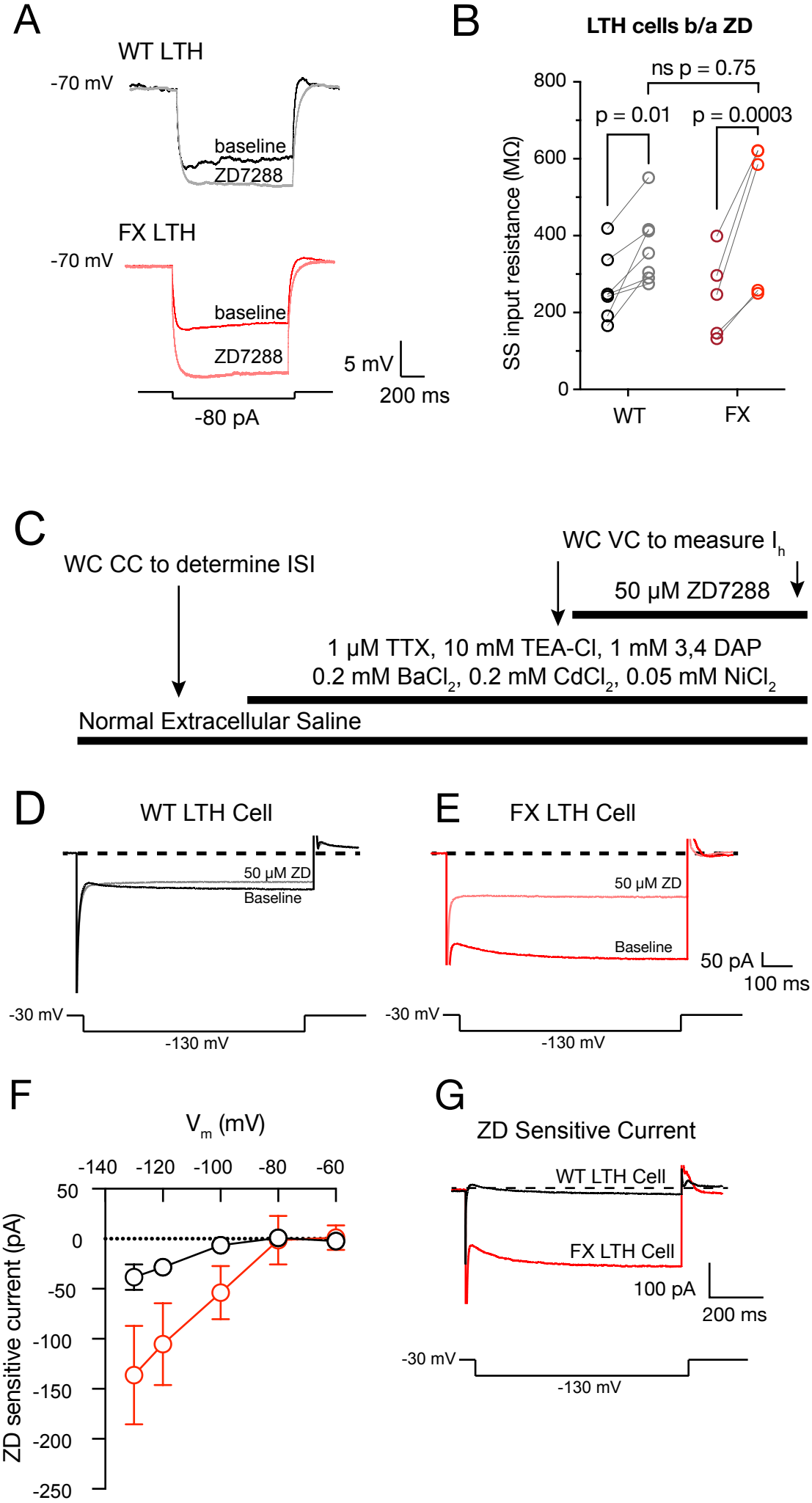
A
WT LTH
-70 mV
baseline
ZD7288
FX LTH
-70 mV
baseline
ZD7288
5 mV
200 ms
-80 pA
B
LTH cells b/a ZD
ns p = 0.75
p = 0.01
p = 0.0003
SS input resistance (MΩ)
800
600
400
200
0
WT
FX
C
WC CC to determine ISI
WC VC to measure $I_h$
50 μM ZD7288
1 μM TTX, 10 mM TEA-Cl, 1 mM 3,4 DAP
0.2 mM $BaCl_2$, 0.2 mM $CdCl_2$, 0.05 mM $NiCl_2$
Normal Extracellular Saline
D
WT LTH Cell
50 μM ZD
Baseline
-30 mV
-130 mV
E
FX LTH Cell
50 μM ZD
Baseline
50 pA
100 ms
-30 mV
-130 mV
F
$V_m$ (mV)
-140
-120
-100
-80
-60
50
0
-50
-100
-150
-200
-250
ZD sensitive current (pA)
G
ZD Sensitive Current
WT LTH Cell
FX LTH Cell
100 pA
200 ms
-30 mV
-130 mV

**Figure 9: FX LTH neurons have more hyperpolarization activated current Ih compared to WT LTH neurons**

a) Traces of WT (black) and FX (red) neurons to a hyperpolarizing step of -80 pA. Post-ZD traces in grey (WT) and pink (FX) b) WT and FX LTH cells show a significant increase in steady-state input resistance in response to Ih channel blocker ZD 7288 (WT: unpaired t-test, $p = 0.005$; FX: unpaired t-test, $p = 0.02$). No difference between WT and FX LTH neurons in input resistance post-ZD application. c) Experimental procedure for whole-cell voltage clamp experiments to measure Ih in WT and FX LTH neurons. d) Current traces of WT LTH neurons in baseline conditions (black) and post-bath application of Ih channel blocker ZD7288 (grey). e) current traces of FX LTH neurons in baseline (red) and post- bath application of ZD7288 (pink). f) FX LTH neurons have higher Ih (two-way ANOVA, main effect of genotype: $F(1,29)=1.107$, $p=0.0005$) g) traces of subtracted ZD sensitive current in WT (black) and FX (red) LTH neurons.